Fault-Tolerant Control of Dual Three-Phase Permanent-Magnet Synchronous Machine Drives Under Open-Phase Faults

Wei Wang, *Member, IEEE*, Jinghao Zhang, Ming Cheng, *Fellow, IEEE*, and Shihua Li, *Senior Member, IEEE*

***Abstract*—In this paper, a fault-tolerant control is proposed for dual three-phase permanent-magnet synchronous machine (PMSM) drives under open-phase faults. The object of the proposed fault-tolerant control is to maximize the torque capacity while the overcurrent protection is taken into account. Hence, the proposed fault-tolerant control is named as torque mode in this paper. Another existed fault-tolerant control for dual three-phase PMSM drives under open-phase faults is loss mode, in which the system copper loss is minimized. Torque mode is compared with loss mode, and two important conclusions are given: 1) loss mode can reduce more copper loss; and 2) torque mode can output more torque. The performances of torque mode and loss mode are verified by experimental results.**

***Index Terms*—dSPACE, dual three-phase motor drive, fault tolerance, open phase, permanent-magnet synchronous machine (PMSM).**

NOMENCLATURE

L_s, R_s	Stator inductance, stator resistance.
p_n	Pole pairs.
$\psi_{\rm PM}$	Permanent magnet flux linkage.
ω_e	Electrical angular speed.
u_x	Phase voltages of the dual three-phase PMSM ($x = a_1, b_1, c_1, a_2, b_2, c_2$).
i_x	Phase currents of the dual three-phase PMSM ($x = a_1, b_1, c_1, a_2, b_2, c_2$).
e_x	Phase back-electromotive forces (EMFs) of the dual three-phase PMSM ($x = a_1, b_1, c_1, a_2, b_2, c_2$).
I_{m1}	Phase current magnitude of PMSM-1.
γ_{b1}	Initial phase angle of i_{b1}.
u_{sd1}, u_{sq1}	d- and q-axis voltage of PMSM-1.
i_{sd1}, i_{sq1}	d- and q-axis current of PMSM-1.
e_{sd1}, e_{sq1}	d- and q-axis back EMF of PMSM-1.
T_{e1}, θ_{e1}	Electromagnetic torque and electrical rotor position of PMSM-1.
u_{sd2}, u_{sq2}	d- and q-axis voltage of PMSM-2.
i_{sd2}, i_{sq2}	d- and q-axis current of PMSM-2.
e_{sd2}, e_{sq2}	d- and q-axis back EMF of PMSM-2.
T_{e2}, θ_{e2}	Electromagnetic torque and electrical rotor position of PMSM-2.
$\Delta\theta$	Phase shift, $\Delta\theta = \theta_{e2} - \theta_{e1}$.
T_e	Total electromagnetic torque.
I_T	Torque current.
$\bar{p}_x$	Average copper losses of phase-x ($x = a_1, b_1, c_1, a_2, b_2, c_2$).
k_x	Per-unit value of $\bar{p}_x$ ($x = b_1, c_1, a_2, b_2, c_2$).
$k_{\max}$	Maximum per-unit average phase copper loss.
$k_{\max\_\min}$	Minimum value of $k_{\max}$.
$p_{\rm Cu}$	System copper loss of the studied dual three-phase PMSM drive system.
$\bar{p}_{\rm Cu}$	Average system copper loss of the studied dual three-phase PMSM drive system.
$\bar{p}_{\rm Cu2}, \bar{p}_{\rm Cu3}, \bar{p}_{\rm Cu4}$	Average system copper losses of OP-2, OP-3, and OP-4, respectively.
$k_{\rm Cu2}, k_{\rm Cu3}, k_{\rm Cu4}$	Per-unit values of $\bar{p}_{\rm Cu2}, \bar{p}_{\rm Cu3}, \bar{p}_{\rm Cu4}$.
η	Current ratio, I_{m1}/I_T.
$I_{\rm rated}$	Rated phase current.
$I_{\rm RMS}$	RMS phase current.

Manuscript received November 4, 2015; revised January 7, 2016 and March 14, 2016; accepted April 24, 2016. Date of publication April 27, 2016; date of current version December 9, 2016. This work was supported in part by the "973 Program" of China (Project 2013CB035603), by the China Postdoctoral Science Foundation (Project: 2015M581697), by the Jiangsu Planned Projects for Postdoctoral Research Funds of China (Project: 1501043B), and by the Fundamental Research Funds for the Central Universities (Project: 2242015K40031). Recommended for publication by Associate Editor J. Zhang.

W. Wang, J. Zhang, and M. Cheng are with the School of Electrical Engineering, Southeast University, Nanjing 210096, China (e-mail: wangwei1986@seu.edu.cn; zhangjinghao369@163.com; mcheng@seu.edu.cn.)

S. Li is with the School of Automation, Southeast University, Nanjing 210096, China (e-mail: lsh @seu.edu. cn)

Color versions of one or more of the figures in this paper are available online at http://ieeexplore.ieee.org.

Digital Object Identifier 10.1109/TPEL.2016.2559498

I. INTRODUCTION

DUE to higher power density and higher efficiency, the permanent-magnet synchronous machine (PMSM) has received more and more attentions recently [1]–[8]. Compared with three-phase motor drives, multiphase motor drives have several significant advantages: reduced torque pulsation, lower power per phase, and higher reliability [9]–[12]. Nowadays, high-power and high-switching-frequency power electronics devices are usually expensive or not available [13]. Therefore, multiphase PMSM drives are very suitable for high-power applications, such as electric vehicles, renewable generation, and ship propulsion. The dual three-phase PMSM is one of the most interesting multiphase motors since it can take full advantages of well-developed three-phase PMSM drives [14]–[16]. One dual three-phase PMSM has two sets of three-phase stator windings spatially shifted by specific electrical degrees with isolated neutral points. To some extent, one dual three-phase PMSM can be treated as two same three-phase PMSMs, and then two three-leg

voltage-source inverters (VSIs) are usually required. According to Estima and Cardoso [17], the failure rate of power electronics devices contributes more than 50% of all the remaining component faults. For the dual three-phase PMSM drive, more power electronics devices mean more failure rate. Among all the faults of motor drives, the open-phase fault is a typical one and it can be caused by power electronics devices or stator windings. Once the single open-phase fault occurs, the traditional solution is to isolate the corresponding three-phase winding set [18]. As a result, the dual three-phase motor is degraded into a three-phase motor. Obviously, this solution will result in a significant reduction of maximum torque. Hence, the fault-tolerant control sometimes is required to enhance the system reliability in critical applications [19], [20].

So far, many fault-tolerant controls have been proposed to cope with open-phase faults. In [21], the neutral point of the three-phase PMSM is connected to the midpoint of two split capacitors by means of a triode for alternating current to keep the continual operation when open-phase faults occur. In the research work of [21], not only the mathematical model of three-phase PMSMs under open-phase faults but also the corresponding vector control strategies are proposed. The split capacitors also can be replaced by a fault-tolerant leg [22], [23]. In [24]–[26], one five-leg VSI is used to control two three-phase motors, in which two phase windings from two different motors share one common leg and the other four phase windings are, respectively, connected to the remaining four legs. In [27] and [28], two three-phase motors are fed by one four-leg VSI, and two phase windings from two different motors are connected to the neutral point of two split capacitors. In [29], two three-phase induction motors are fed by single three-leg VSI and a weighted control is specially designed. Generally, to use the abovementioned fault-tolerant controls, extra hardware devices are usually required [21]–[29], which will increase the system cost and complexity. In [30], a fault-tolerant control is proposed for the dual three-phase PMSM drive to minimize the system copper loss, in which there are no additional components and open-phase faults are taken into account. However, only the system copper loss is discussed in [30] while phase copper losses are ignored. As is known, the phase copper loss plays an important role in the design of the overcurrent protection, and the ignorance of phase copper losses will make PMSM drives dangerous. Unfortunately, to the best of authors' knowledge, the phase copper loss has not been analyzed and no corresponding fault-tolerant control has been proposed for dual three-phase PMSM drives under open-phase faults.

In this paper, a fault-tolerant control is proposed for dual three-phase PMSM drives under open-phase faults to maximize the torque capacity, in which the maximum phase copper loss is evaluated. Hence, the proposed fault-tolerant control is named as torque mode. Torque mode is compared with another existed fault-tolerant mode (loss mode) while loss mode can minimize the system copper loss. This paper is organized as follows. The studied dual three-phase PMSM drive system is defined in Section II. Loss mode is presented in Section III. Torque mode is proposed in Section IV. Loss mode and torque mode are compared in Section V. Some experiments are carried out in Section VI to verify the comparisons. Finally, some conclusions are drawn in Section VII.

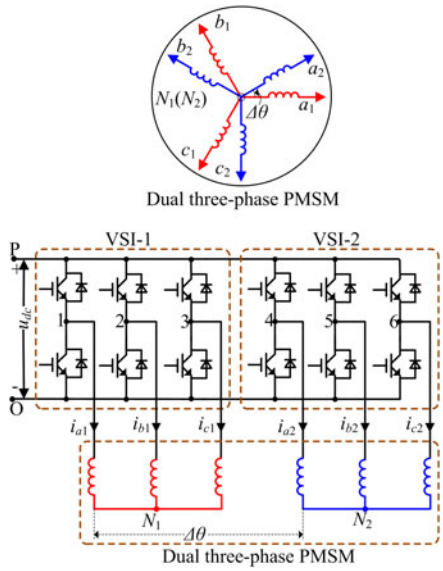

Fig. 1. Studied dual three-phase PMSM drive.

II. Studied Dual Three-Phase PMSM Drive

The studied dual three-phase PMSM drive is illustrated in Fig. 1, which consists of one surfaced-mounted dual three-phase PMSM, two VSIs, and one common dc bus. The six phases of the studied dual three-phase PMSM are, respectively, defined as phase-$a1$, phase-$b1$, phase-$c1$, phase-$a2$, phase-$b2$, and phase-$c2$. The studied dual three-phase PMSM is divided into two winding sets (PMSM-1 and PMSM-2), and they have independent neutral points (N_1 and N_2). The first winding set PMSM-1 contains phase-$a1$, phase-$b1$, and phase-$c1$, while phase-$a2$, phase-$b2$, and phase-$c2$ belong to the second winding set PMSM-2.

Four operation modes are defined in this paper. It should be pointed out that both OP-3 and OP-4 belong to the fault-tolerant operation.

1) *OP-1 (normal mode):* Two winding sets are healthy.
2) *OP-2 (isolated mode):* when one power switch is opened, all the other five power switches of the faulty winding set are switched off and the healthy winding set is still used.
3) *OP-3 (loss mode):* when one power switch is opened, the other power switch of the faulty leg is switched off and the five healthy legs are used; the system copper loss is minimized.
4) *OP-4 (torque mode):* its system topology is as same as that of loss mode; the maximum phase copper loss is minimized, and the torque capacity is maximized.

According to [30], the total torque can be calculated by (1) since the studied dual three-phase PMSM is surface mounted

$$\begin{cases} T_{e1} = 1.5\, p_n \psi_{\mathrm{PM}} i_{sq1} \\ T_{e2} = 1.5\, p_n \psi_{\mathrm{PM}} i_{sq2} \\ T_e = T_{e1} + T_{e2}. \end{cases} \tag{1}$$

It is assumed that phase-$a1$ is opened under open-phase faults, i. e., $i_{a1}=0$ and $i_{b1}=-i_{c1}$.i_{b1} is defined as follows:

$$i_{b1}=I_{m1}\cos(\theta_{e1}+\gamma_{b1}). \tag{2}$$

According to the Park transformation (3), i_{sd1} and i_{sq1} can be calculated in (4)

$$\boldsymbol{P}_{3/2}(\theta) = \frac{2}{3}\begin{bmatrix}\cos(\theta) & \cos(\theta-2\pi/3) & \cos(\theta+2\pi/3)\\ -\sin(\theta) & -\sin(\theta-2\pi/3) & -\sin(\theta+2\pi/3)\\ 0.5 & 0.5 & 0.5\end{bmatrix} \tag{3}$$

$$\begin{cases} i_{sd1}=\dfrac{I_{m1}}{\sqrt{3}}\left[\sin(2\,\theta_{e1}+\gamma_{b1})-\sin\gamma_{b1}\right]\\ i_{sq1}=\dfrac{I_{m1}}{\sqrt{3}}\left[\cos(2\,\theta_{e1}+\gamma_{b1})+\cos\gamma_{b1}\right]. \end{cases} \tag{4}$$

According to (4), the average torque of PMSM-1 can be maximized by setting γ_{b1} as 0. Hence, (4) can be simplified as

$$\begin{cases} i_{sd1}=\dfrac{I_{m1}}{\sqrt{3}}\sin2\,\theta_{e1}\\ i_{sq1}=\dfrac{I_{m1}}{\sqrt{3}}\left(\cos2\,\theta_{e1}+1\right). \end{cases} \tag{5}$$

It can be seen from (5) that the double-frequency torque ripple appears. To compensate torque ripples and reduce the copper loss, i_{sd2} and i_{sq2} are, respectively, set as

$$\begin{cases} i_{sd2}=0\\ i_{sq2}=I_T-\dfrac{I_{m1}}{\sqrt{3}}(1+\cos2\,\theta_{e1}) \end{cases} \tag{6}$$

with

$$I_T=\frac{T_e}{1.5p_n\psi_{\rm PM}}. \tag{7}$$

III. Loss Mode

As is well-known, the system copper loss of the studied drive system

$$p_{\rm Cu}=1.5\,R_s[(i_{sd1}^2+i_{sq1}^2)+(i_{sd2}^2+i_{sq2}^2)]. \tag{8}$$

For a nonzero rotor speed, the average value of the system copper loss in the fault-tolerant operation can be calculated by substituting (5) and (6) into (8)

$$\bar{p}_{\rm Cu}=1.5\,I_T^2R_s\left(\frac{7}{6}\eta^2-2\eta/\sqrt{3}+1\right). \tag{9}$$

The per-unit value of $\bar{p}_{\rm Cu}$ is defined as follows:

$$k_{\rm Cu}=\frac{\bar{p}_{\rm Cu}}{0.5\,I_T^2R_s}=3.5\eta^2-2\sqrt{3}\eta+3. \tag{10}$$

According to the analysis in [30], $k_{\rm Cu}$ is minimized when

$$\eta=2\sqrt{3}/7. \tag{11}$$

It should be pointed out here that the coefficient of Park transformation in this paper is different from that in [30]. That is why η is $2\sqrt{2}/7$ in [30]. However, their final effects are same.

IV. Torque Mode

In this section, torque mode is proposed for the studied dual three-phase PMSM drive system.

A. Calculation of Phase Copper Loss

In normal and isolated modes, all used phase windings have same copper losses. To find out the actual situation of phase copper losses in fault-tolerant mode, all average phase copper losses are calculated in (12) by Park inverse transformation shown in (13)

$$\begin{cases} \bar{p}_{\,b1}=\bar{p}_{\,c1}=\overline{i_{\,c1}^{\,2}}R_{\,s}=0.5\,\eta^2I_{\,T}^{\,2}R_{\,s}\\ \bar{p}_{\,a2}=\overline{i_{\,a2}^{\,2}}R_{\,s}=\dfrac{I_{\,T}^{\,2}R_{\,s}}{12}\{[3-2\cos(2\Delta\theta)]\eta^2\\ \qquad -2\sqrt{3}[2-\cos(2\Delta\theta)]\eta+6\}\\ \bar{p}_{\,b2}=\overline{i_{\,b2}^{\,2}}R_{\,s}=\dfrac{I_{\,T}^{\,2}R_s}{12}\{[3-2\cos(2\Delta\theta+2\pi/3)]\eta^2\\ \qquad -2\sqrt{3}[2-\cos\left(2\Delta\theta+2\pi/3\right)]\eta+6\}\\ \bar{p}_{\,c2}=\overline{i_{\,c2}^{\,2}}R_{\,s}=\dfrac{I_{\,T}^{\,2}R_{\,s}}{12}\{[3-2\cos(2\Delta\theta\\ \qquad -2\pi/3)]\eta^2-2\sqrt{3}[2-\cos(2\Delta\theta-2\pi/3)]\eta+6\} \end{cases} \tag{12}$$

$$\boldsymbol{P}_{2/3}(\theta)=\begin{bmatrix}\cos(\theta) & -\sin(\theta)\\ \cos(\theta-2\pi/3) & -\sin(\theta-2\pi/3)\\ \cos(\theta+2\pi/3) & -\sin(\theta+2\pi/3)\end{bmatrix}. \tag{13}$$

To simplify the analysis, several per-unit values are defined in (14). Two special situations of (14) are illustrated in Fig. 2. It can be seen from Fig. 2 that the five used phase windings do not have same average copper losses, which is an important theoretical basis of the proposed fault-tolerant control

$$\begin{cases} k_{b1}=k_{c1}=\dfrac{\bar{p}_{b1}}{0.5I_T^2R_s}=\eta^2\\ k_{a2}=\dfrac{\bar{p}_{a2}}{0.5I_T^2R_s}=\dfrac{1}{6}\{[3-2\cos(2\Delta\theta)]\eta^2\\ \qquad -2\sqrt{3}[2-\cos(2\Delta\theta)]\eta+6\}\\ k_{b2}=\dfrac{\bar{p}_{b2}}{0.5I_T^2R_s}=\dfrac{1}{6}\{[3-2\cos(2\Delta\theta+2\pi/3)]\eta^2\\ \qquad -2\sqrt{3}[2-\cos(2\Delta\theta+2\pi/3)]\eta+6\}\\ k_{c2}=\dfrac{\bar{p}_{c2}}{0.5I_T^2R_s}=\dfrac{1}{6}\{[3-2\cos(2\Delta\theta-2\pi/3)]\eta^2\\ \qquad -2\sqrt{3}[2-\cos(2\Delta\theta-2\pi/3)]\eta+6\}. \end{cases} \tag{14}$$

B. Overcurrent Protection

In motor drives, the overcurrent protection is usually designed according to the rated phase current $I_{\rm rated}$. When the actual RMS phase current is greater than the rated phase current, it means that the overload operation occurs. Considering

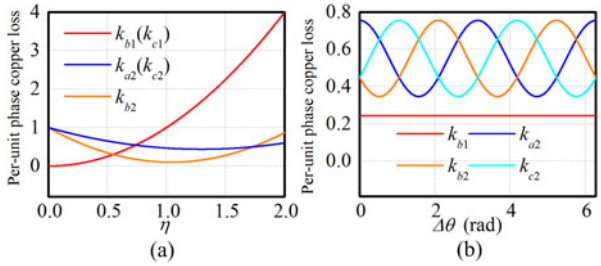

Fig. 2. Curve of per-unit average phase copper losses: (a) $\Delta\theta = \pi/6$ and (b) $\eta = 2\sqrt{3}/7$.

the system safety, the PMSM drives cannot run in the overload condition for a long time and the overcurrent protection should be activated. The square of the RMS phase current I_{RMS}^2 is proportional to the phase copper loss $I_{\mathrm{RMS}}^2 R_s$. Therefore, the definition of the overload operation also can be changed as follows: the actual phase copper loss $I_{\mathrm{RMS}}^2 R_s$ is greater than the rated phase copper loss $I_{\mathrm{rated}}^2 R_s$. Therefore, the phase copper loss is used to check whether the motor drive is in the overload operation and whether the overcurrent protection should be activated.

In normal and isolated mode, all used phase windings have same copper losses. It is easy to obtain all phase copper losses by equally dividing the system copper loss and implement the overcurrent protection. However, it becomes difficult for two fault-tolerant modes (loss mode and torque mode) since their average phase copper losses are not same, as shown in Fig. 2. Hence, the maximum average phase copper loss cannot be greater than the rated phase copper loss for a long time. The problem has become how to find the maximum average phase copper loss. Fig. 2 just provides two special situations and the common analysis should be carried out.

C. Maximum Torque Capacity

By differentiating (14), two monotonic intervals are obtained:

1) k_{b1}, k_{a2}, k_{b2}, and k_{c2} are monotonic increasing, $\eta \in (\sqrt{3}, +\infty)$;
2) k_{b1}, k_{a2}, k_{b2}, and k_{c2} are monotonic decreasing, $\eta \in (-\infty, 0)$.

As an example, the monotonicity of k_{a2} is verified by Fig. 3. The per-unit maximum phase copper loss $k_{\max}$ is defined as

$$k_{\max} = \max\{k_{b1}, k_{a2}, k_{b2}, k_{c2}\}. \tag{15}$$

The surface diagram of $k_{\max}$ is illustrated in Fig. 4. In order to maximize the torque capacity, $k_{\max}$ should be minimized. For a known phase shift $\Delta\theta$, the value of η can be changed by regulating I_{m1} since the value of I_T has been determined by the torque command according to (7). The problem has become how to find the minimized value of $k_{\max}$, which is defined as

$$k_{\max\_\min} = \min\{k_{\max}, \eta \in \boldsymbol{R}\}. \tag{16}$$

According to two monotonic intervals $(\sqrt{3}, +\infty)$ and $(-\infty, 0)$, $k_{\max\_\min}$ can be obtained in the value interval $[0, \sqrt{3}]$,

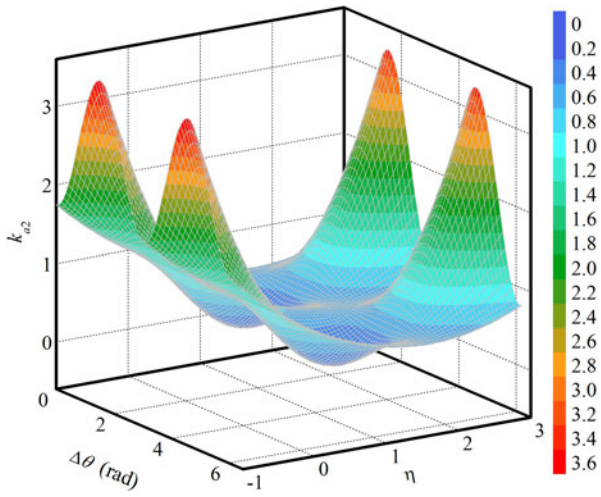

Fig. 3. Surface diagram of k_{a2} in torque mode.

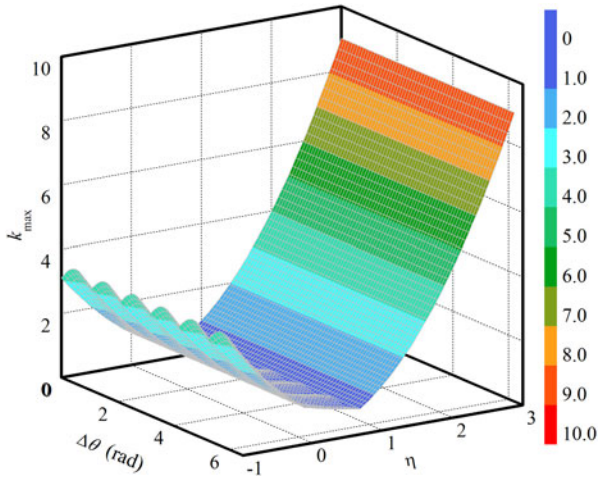

Fig. 4. Surface diagram of $k_{\max}$ in torque mode.

which is verified by Fig. 4. Hence, (16) can be further modified as

$$k_{\max\_\min} = \min\{k_{\max}, \eta \in [0, \sqrt{3}]\}. \tag{17}$$

According to the definition, $k_{\max\_\min}$ is the maximum value among k_{b1}, k_{a2}, k_{b2}, and k_{c2}. Except k_{b1}, the expressions of k_{a2}, k_{b2}, and k_{c2} are complex since all of them contain two variables $(\Delta\theta, \eta)$ and trigonometric functions. Therefore, it is difficult to derive a convergent solution for $k_{\max\_\min}$ from (14)–(17) and the data-fitting method is finally employed in this paper. The curve of $k_{\max\_\min}$ is illustrated in Fig. 5. At a given $\Delta\theta$, $k_{\max\_\min}$ is obtained when $\eta = \eta_{\max\_\min}$.

According to Fig. 5, a formula can be obtained by the data-fitting method

$$k_{\max\_\min} = 0.4422 + 0.202\cos 2\alpha \tag{18}$$

$$\eta_{\max\_\min} = 0.672 + 0.13\cos 2\alpha \tag{19}$$

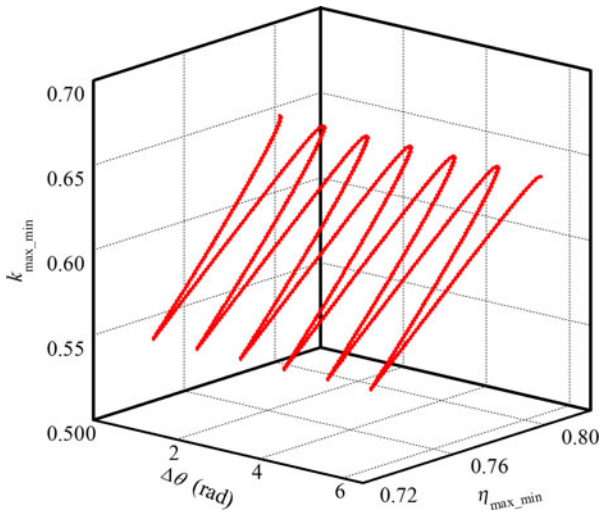

Fig. 5. Curves of $\eta_{\max\_\min}$ and $k_{\max\_\min}$ in torque mode.

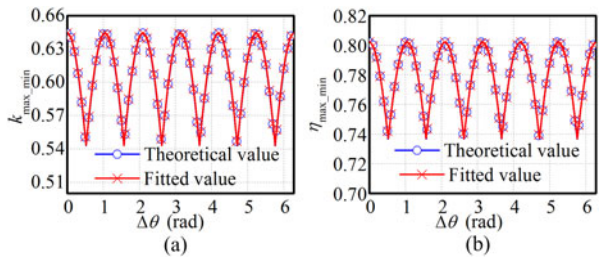

Fig. 6. Comparisons between the theoretical values and fitted values: (a) $k_{\max\_\min}$ and (b) $\eta_{\max\_\min}$.

with

$$\alpha = \left[\left(\Delta\theta + \frac{\pi}{6}\right) \bmod \frac{\pi}{3}\right] - \frac{\pi}{6}. \tag{20}$$

The theoretical values of $k_{\max\_\min}$ and $\eta_{\max\_\min}$ deduced from Fig. 5, and the fitted values of $k_{\max\_\min}$ and $\eta_{\max\_\min}$ calculated by (18) and (19), are compared in Fig. 6. It can be seen from Fig. 6 that the theoretical values and the fitted values are overlapped, which verifies the high precision of (18) and (19). Hence, (18) can be used to calculate the minimized maximum average phase copper loss and the corresponding $\eta_{\max\_\min}$ can be determined by (19). The feature of torque mode is $\eta = \eta_{\max\_\min}$ while the feature of loss mode is $\eta{=}2\sqrt{3}/7$. According to (19), the value range of $\eta_{\max\_\min}$ is [0.542, 0.802], which does not contain $2\sqrt{3}/7$. Therefore, torque mode and loss mode are two totally independent operation modes.

V. Performance Analysis

In this section, three postfault operations (isolated mode, loss mode, torque mode) are compared in three aspects: copper loss, torque capacity, and temperature effect.

A. Copper Loss

The curve of $k_{\max}$ under the condition (11) is illustrated in Fig. 7 and the curve can be represented by (21), which is

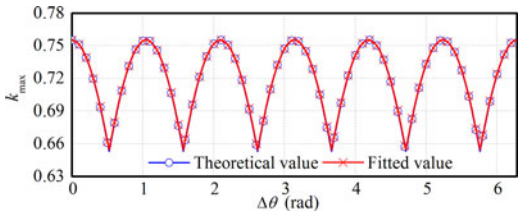

Fig. 7. Curve of $k_{\max}$ in loss mode.

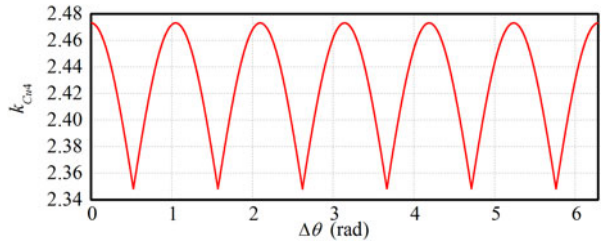

Fig. 8. Curve of k_{Cu4}.

obtained by the data-fitting method

$$k_{\max} = 0.5537 + 0.2014\cos 2\alpha. \tag{21}$$

In isolated mode, η is 0. According to (10), the corresponding per-unit average system copper loss k_{Cu2} is 3.

In loss mode, according to (10) and (11), the corresponding per-unit average system copper loss k_{Cu3} is 15/7.

In torque mode, according to (10) and Fig. 6(b), the corresponding per-unit average system copper loss k_{Cu4} is illustrated in Fig. 8.

Compared with k_{Cu2}, k_{Cu3} is reduced by 28.57% while k_{Cu4} is decreased from 17.67%–21.67%. Obviously, loss mode can save more energy. It means the value of k_{Cu2} and k_{Cu3} are not affected by the phase shift $\Delta\theta$. On the other hand, k_{Cu4} depends on the value of $\Delta\theta$.

B. Torque Capacity

In this subsection, the overcurrent protection is taken into account. For one healthy winding set, the maximum torque capacity is defined as $T_{\max}$. Hence, the maximum value of I_T can be calculated as

$$I_{\max} = \frac{T_{\max}}{1.5\, p_n \psi_{\mathrm{PM}}}. \tag{22}$$

In isolated mode, the corresponding maximum torque $T_{\max 2}$ is $T_{\max}$.

In loss mode, the corresponding maximum torque $T_{\max 3}$ is obtained when the maximum average phase copper loss is equal to $0.5I_{\max}^2 R_s$. The maximum phase copper loss can be calculated from (21), i.e.,

$$(0.5537 + 0.2014\,\cos 2\alpha) \times 0.5 I_{\max 3}^2 R_s = 0.5 I_{\max}^2 R_s.$$

By solving the above equation, the following condition can be obtained:

$$I_{\max 3} = \frac{I_{\max}}{\sqrt{0.5537 + 0.2014\cos 2\alpha}}. \tag{23}$$

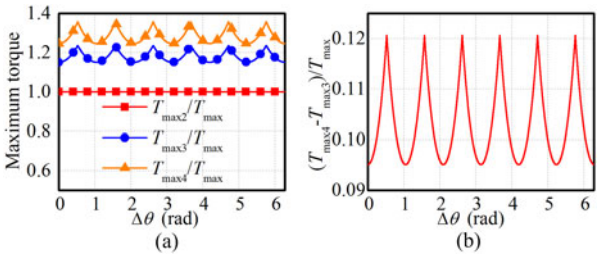

Fig. 9. Comparison of three maximum torques: (a) torque ratio curves and (b) torque ratio error.

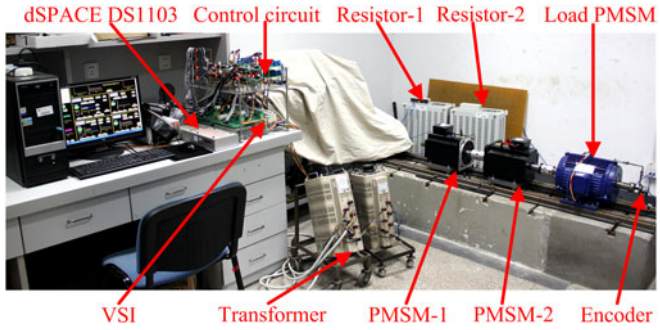

Fig. 10. Experiment platform.

According to (7), $T_{\max 3}$ can be calculated from (23)

$$T_{\max 3} = \frac{T_{\max}}{\sqrt{0.5537 + 0.2014\cos 2\alpha}}. \tag{24}$$

In torque mode, the corresponding maximum torque $T_{\max 4}$ is also obtained when the maximum average phase copper loss is equal to $0.5I_{\max}^2 R_s$. The maximum phase copper loss can be calculated from (18), i.e.,

$$(0.4422 + 0.202\cos 2\alpha) \times 0.5I_{\max 4}^2 R_s = 0.5I_{\max}^2 R_s.$$

By solving the above equation, the following condition can be similarly obtained:

$$I_{\max 4} = \frac{I_{\max}}{\sqrt{0.4422 + 0.202\cos 2\alpha}}. \tag{25}$$

According to (7), $T_{\max 4}$ can be calculated from (25)

$$T_{\max 4} = \frac{T_{\max}}{\sqrt{0.4422 + 0.202\cos 2\alpha}}. \tag{26}$$

$T_{\max 2}/T_{\max}, T_{\max 3}/T_{\max}, T_{\max 4}/T_{\max}$ are illustrated in Fig. 9. Compared with $T_{\max 2}, T_{\max 3}$ is increased from 15.1%–23.6% while $T_{\max 4}$ is increased from 24.6%–35.7%. Obviously, torque mode can provide more torque.

C. Temperature Effect

The phase copper loss is decided by both the RMS phase current and the stator resistance. As is known, larger RMS phase current will result in higher temperature and higher temperature will increase the stator resistance. At last, the higher resistance will result in higher phase copper loss. In a word, larger RMS phase current will result in higher phase copper loss considering the temperature effect of the stator resistance. All phase windings have same stator resistances if the stator temperature is same. Due to different phase copper losses, however, the stator temperature of the two winding sets will be different in the single phase open fault. The different stator temperature will make the stator resistances of the five used phase windings different, which will have an effect on the estimation of $k_{\max\_\min}$. However, (14) will become very complex since all the stator resistances cannot be eliminated. To simplify the analysis, it is assumed that the stator resistances remain unchanged and all the stator resistances of the five used phase windings are same. Based on this assumption, (14) becomes simple. The control target of torque mode is to minimize the maximum phase copper loss by setting η as $\eta_{\max\_\min}$. A doubt appears whether this assumption will affect the control target of torque mode. However, this doubt is unnecessary, which will be explained here. According to (14), k_{b1}, k_{a2}, k_{b2}, and k_{c2} also can be considered as the definition of the square of the per-unit RMS phase currents. The calculation procedure of $k_{\max\_\min}$ also can be considered to minimize the maximum RMS phase current. Hence, the minimized maximum RMS phase current can be achieved by setting η as $\eta_{\max\_\min}$, which is not affected by the stator temperature at all. As is analyzed at the beginning of this subsection, lager RMS phase current will result in higher phase copper loss. Therefore, the minimized maximum RMS phase current can result in the minimized maximum phase copper loss, which is the control target of torque mode.

TABLE I
PARAMETERS OF TRACTION PMSM

Parameter	Value
Rated power	5.5 kW
Rated line voltage	380 V
Rated phase current	11 A
Stator resistance R_s	0.625 Ω
Stator inductance L_s	8.5 mH
Permanent magnet flux ψ_{PM}	0.442 Wb
Number of pole pairs P_n	4
Rated speed	1 500 r/min

VI. EXPERIMENTAL VALIDATION

To verify the effectiveness of the proposed fault-tolerant control, an experiment platform is developed, as shown in Fig. 10. For a specific dual three-phase PMSM, the phase shift $\Delta\theta$ is constant. In order to show the universality of the proposed fault-tolerant control, two same surface-mounted three-phase traction PMSMs are coupled together to simulate a dual three-phase PMSM. Based on this special designing, different phase shifts can be provided. The parameters of two three-phase traction PMSMs are listed in Table I. The load is provided by one 5.5-kW PMSM with an encoder of 1024 pulses per revolution. The load is realized by the closed-loop torque control of the load PMSM using the field-oriented control (FOC). The dc bus voltage is 250 V.

The control program is implemented in a dSPACE DS1103 controller. The inputs for the dSPACE DS1103 controller are the measured phase currents and dc bus voltage, and the feed-

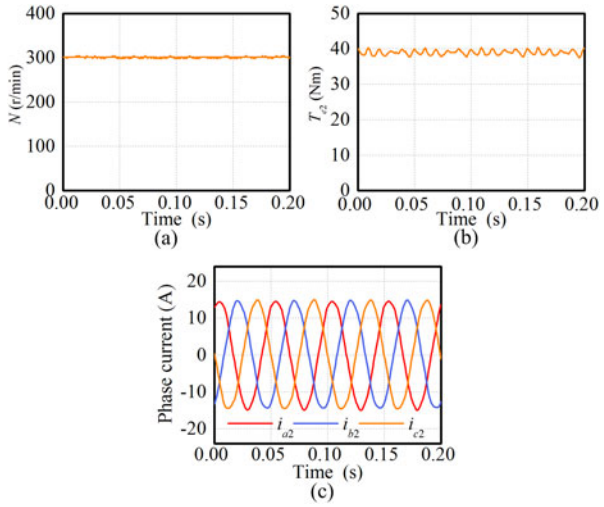

Fig. 11. Experimental results of Experiment 1: (a) speed; (b) torque; and (c) phase currents.

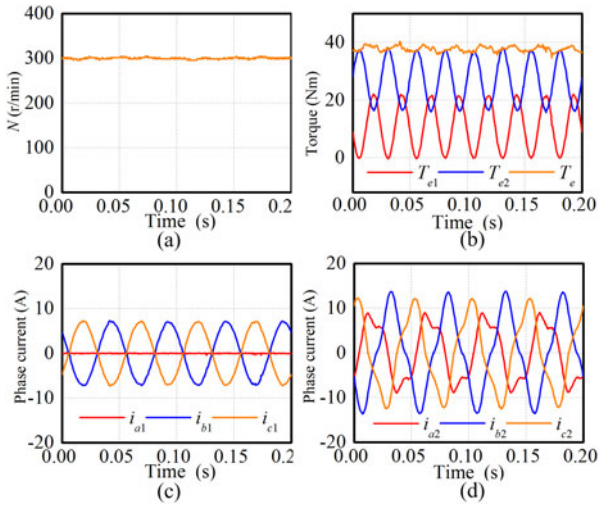

Fig. 12. Experimental results of Experiment 2 in loss mode: (a) speed; (b) torque; (c) phase currents of PMSM-1; and (d) phase currents of PMSM-2.

back signal of the encoder. The switch states for the VSIs are generated by the dSPACE DS1103 controller. A personal computer is employed for editing the control program and commanding the dSPACE DS1103 controller. The switching frequency is 5 kHz and the sampling frequency is 20 kHz. The load torque is 35 N·m. Four experiments are carried out as follows.

A. Experiment 1

In this experiment, the studied dual three-phase PMSM drive system is in the isolated mode, in which PMSM-1 is isolated while PMSM-2 is still used. The experimental results are illustrated in Fig. 11. In the steady state, the system copper loss $\bar{p}_{\mathrm{Cu2}}$ is 201.28 W and the maximum average phase copper loss is 67.58 W.

B. Experiment 2

In this experiment, phase-$a1$ is opened and the other phase windings are used. The phase shift $\Delta\theta$ is 0.4354 rad. Loss mode and torque mode are, respectively, executed, and their experimental results are illustrated in Figs. 12 and 13. The average copper losses of the studied drive system in the steady state are listed in Table II. The average system copper loss of loss mode and torque mode are 135.42 and 153.03 W. Compared with the system copper loss (201.28 W) of Experiment 1, the former (135.42 W) and the latter (153.03 W) are reduced by 32.72% and 23.93%, respectively. The maximum average phase copper losses of loss mode and torque mode are 43.87 and 38.09 W, respectively. Compared with the maximum average phase copper loss (67.58 W) of Experiment 1, the former (43.87 W) and the latter (38.09 W) are reduced by 35.08% and 43.64%, respectively. As a result, the maximum torques of loss mode and torque mode are increased by 24.12% and 33.20%, respectively. The experimental results verify the analysis in Section V.

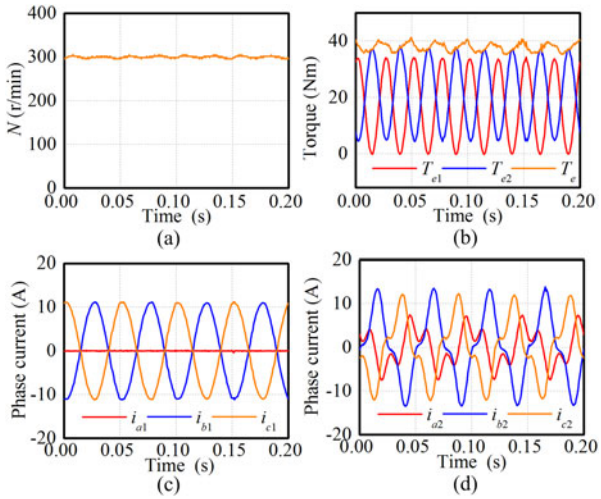

Fig. 13. Experimental results of Experiment 2 in torque mode: (a) speed; (b) torque; (c) phase currents of PMSM-1; and (d) phase currents of PMSM-2.

C. Experiment 3

Without special declaration, the experiment conditions are as same as those of Experiment 2. The only difference is that $\Delta\theta$ becomes 5.7280 rad. The experimental results of loss mode and torque mode are illustrated in Figs. 14 and 15, respectively. The copper losses of the studied dual three-phase PMSM drive system in the steady state are listed in Table III. The average system copper loss (135.15 W) of loss mode is very close to the corresponding value (135.45 W) of Experiment 2, which verifies the analysis in Section V that k_{Cu3} is not affected by $\Delta\theta$. The maximum average phase copper loss (47.56 W) of loss mode is different from the corresponding value (43.87 W) of Experiment 2, which verifies the analysis in (24) that T_{max3} is affected by $\Delta\theta$. The average system copper loss (155.63 W) of torque mode is different from the corresponding value (153.03 W) of Experiment 2, which verifies the analysis in

TABLE II
COPPER LOSSES OF EXPERIMENT 2

	Average copper loss (W)	
	Loss mode	Torque mode
Phase-*b*1	15.63	38.09
Phase-*c*1	15.63	38.07
Phase-*a*2	22.14	10.30
Phase-*b*2	43.87	37.02
Phase-*c*2	38.16	29.56
Maximum value	43.87	38.09
Total	135.42	153.03

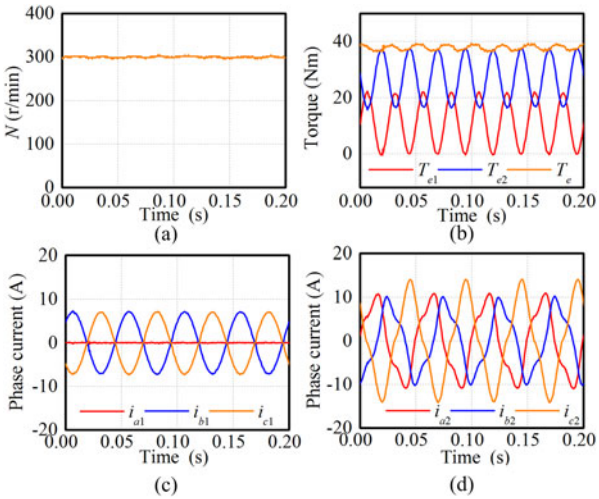

Fig. 14. Experimental results of Experiment 3 in loss mode: (a) speed; (b) torque; (c) phase currents of PMSM-1; and (d) phase currents of PMSM-2.

TABLE III
COPPER LOSSES OF EXPERIMENT 3

	Average copper loss (W)	
	Loss mode	Torque mode
Phase-*b*1	15.61	40.38
Phase-*c*1	15.61	40.37
Phase-*a*2	31.71	21.31
Phase-*b*2	24.66	12.91
Phase-*c*2	47.56	40.66
Maximum value	47.56	40.66
Total	135.15	155.63

Section V that $k_{\mathrm{Cu}4}$ is affected by $\Delta\theta$. The maximum phase copper loss (40.66 W) of torque mode is also different from the corresponding value (38.09 W) of Experiment 2, which verifies the analysis in (26) that $T_{\max 4}$ is affected by $\Delta\theta$.

D. Experiment 4

In this experiment, the reference speed is set as 600 r/min and the other experimental parameters are as same as those in Experiment 2. Four operation modes (normal mode, isolated mode, torque mode, loss mode) are verified in Experiment 4 and the experimental results are shown in Fig. 16, in which not only

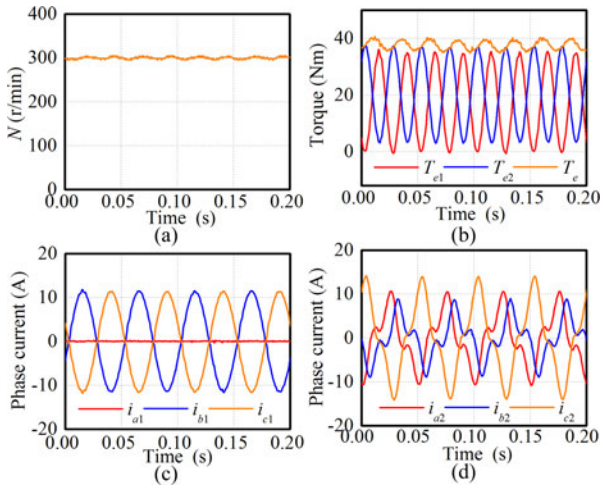

Fig. 15. Experimental results of Experiment 3 in torque mode: (a) speed; (b) torque; (c) phase currents of PMSM-1; and (d) phase currents of PMSM-2.

TABLE IV
COPPER LOSSES OF EXPERIMENT 4

	Average copper loss (W)			
	Normal mode	Isolated mode	Torque mode	Loss mode
Phase-*a*1	21.90	0	0	0
Phase-*b*1	22.10	0	53.92	23.12
Phase-*c*1	22.99	0	53.90	23.15
Phase-*a*2	22.12	92.14	11.70	28.65
Phase-*b*2	22.64	93.85	53.44	63.75
Phase-*c*2	22.19	93.02	46.86	58.36
Maximum value	22.99	93.85	53.92	63.75
Total	133.93	279.01	219.82	197.04

steady state but also transient experimental results are illustrated. The experimental results shown in Fig. 16 can be divided into four regions: normal mode (0–3.74 s), isolated mode (3.74–8.56 s), torque mode (8.56–12.84 s), and loss mode (12.84–16.00 s). The copper losses in these four regions are listed in Table IV. Comparing with Experiment 1, the total copper loss of isolated mode in Experiment 4 is increased by 38.81%. Similarly, all the corresponding copper losses of torque and loss mode in Table IV are also nearly increased by 38.81% through comparing with Table II. The increase of the copper losses is due to the increase of power output since the speed has been doubled in Experiment 4. Therefore, the conclusions obtained from Experiment 1 and Experiment 2 also can be verified by Experiment 4. Comparing with normal mode, the total copper loss of isolated mode is doubled and the phase copper loss is even increased by 400%, which are verified by Table IV. Due to the significant increase of phase copper loss, sometimes isolated mode cannot be used if the load is heavy. Even though the significant ripples of currents and torques appear during the switching procedures among different operation modes, the duration is so short that the influences nearly can be neglected, which have been verified by the smooth speed profile in Fig. 16. A feature should be pointed out that the torque ripples become

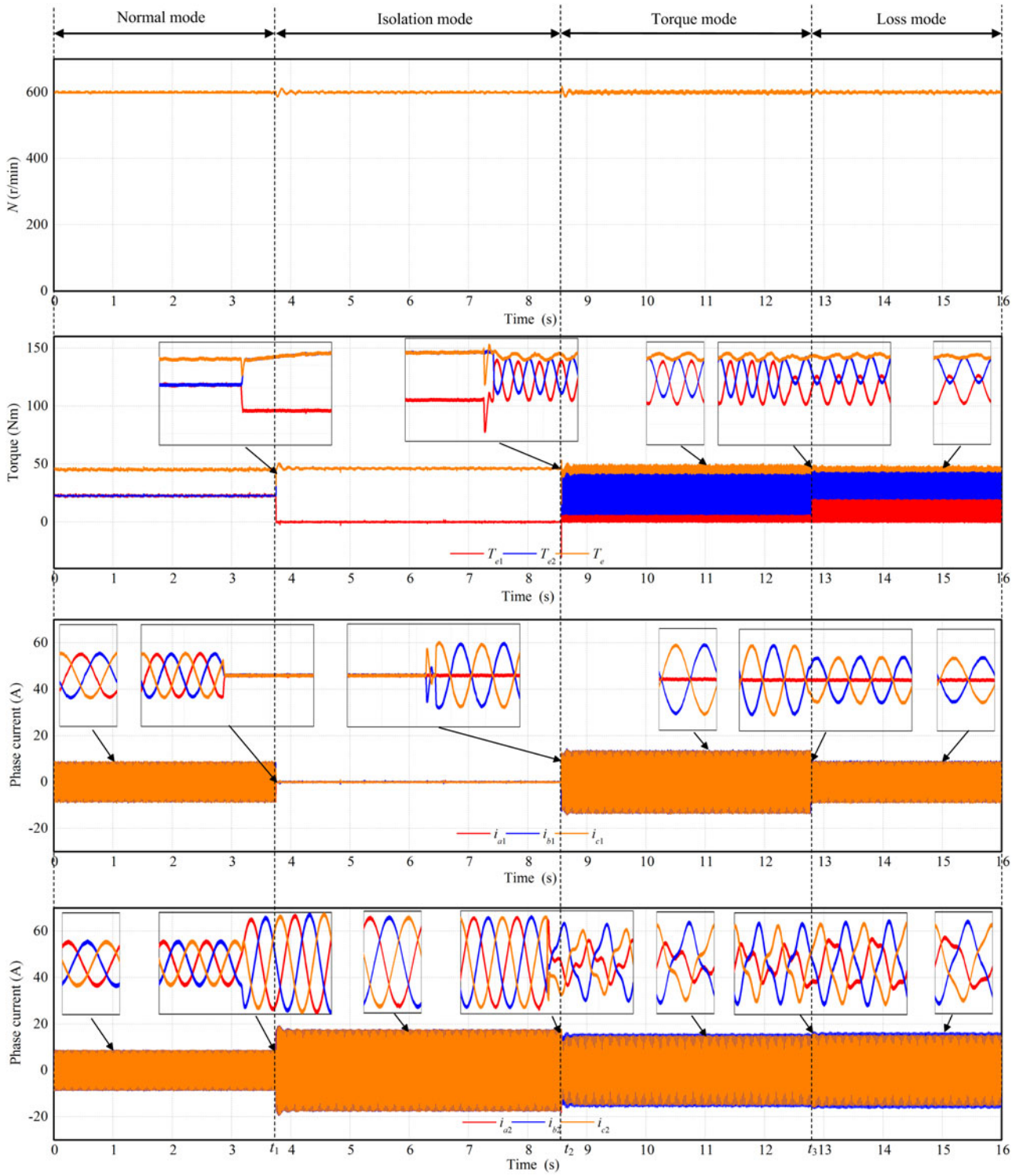

Fig. 16. Experimental results of Experiment 4: (a) speed; (b) torque; (c) phase currents of PMSM-1; and (d) phase currents of PMSM-2.

larger in fault-tolerant mode especially in torque mode. When one phase is open, three operation modes (isolated mode, torque mode, loss mode) can be selected to remain continual operation and their features are listed in Table V. The final selection is based on the requirement of the dual three-phase PMSM drive system.

VII. Conclusion

In this paper, a fault-tolerant control is proposed for dual three-phase PMSM drives under open-phase faults. The contributions of this paper can be summarized as follows.

a) The formulas of the maximum average phase copper loss in loss mode and torque mode are, respectively, developed

TABLE V
FEATURES OF THREE FAULT-TOLERANT OPERATION MODES

Operation mode	Torque capacity	Torque ripple	Copper loss
Isolated mode	Small	Small	Large
Loss mode	Medium	Medium	Small
Torque mode	Large	Large	Medium

by the data-fitting method. The fitted formulas are high reliable since no motor parameters are used. According to the fitted formula, the overcurrent phenomenon can be avoided.

b) If the load is light, loss mode is preferable since the total copper loss can be reduced by 28.57%. Loss mode may extend the drive distance or the operation time. This point is important for the applications where the onboard energy is very limited, such as electric vehicles.

c) If loss mode cannot provide enough torque, torque mode should be activated since the total torque can be increased by 24.6%–35.7%. Otherwise, the dual three-phase PMSM drive system will be forced to halt and must wait for help. By using torque mode, the torque capacity can be maximized to avoid forced halt as much as possible.

d) The influence of the phase shift is evaluated for the proposed fault-tolerant control.

e) All the analyses are verified by experimental results.

Even though the proposed fault-tolerant control is designed for dual three-phase PMSM drives, it also can be used for dual motor drives if two motors share one common rigid shaft.

APPENDIX

A. Calculation Procedure of (9)

Substituting (5) and (6) into (8) gives

$$p_{\mathrm{Cu}} = \frac{3}{2}R_s\left\{\frac{1}{3}I_{m1}^2[(\sin 2\theta_{e1})^2+(\cos 2\theta_{e1}+1)^2] + \left[I_T-\frac{1}{\sqrt{3}}I_{m1}(1+\cos 2\theta_{e1})\right]^2\right\}. \tag{A-1}$$

As is known, $\eta = I_{m1}/I_T$. Therefore, (A-1) can be simplified as (A-2), which can be further simplified as (A-3)

$$p_{Cu} = \frac{3}{2}I_T^2R_s\left\{\frac{1}{3}\eta^2[(\sin 2\theta_{e1})^2+(\cos 2\theta_{e1}+1)^2] + \left[1-\frac{1}{\sqrt{3}}\eta(1+\cos 2\theta_{e1})\right]^2\right\} \tag{A-2}$$

$$p_{Cu} = \frac{3}{2}I_T^2R_s\left[\left(\frac{7}{6}\eta^2-\frac{2}{\sqrt{3}}\eta+1\right) + \left(\frac{4}{3}\eta^2-\frac{2}{\sqrt{3}}\eta\right)\cos 2\theta_{e1}+\frac{1}{6}\eta^2\cos 4\theta_{e1}\right]. \tag{A-3}$$

For a nonzero rotor speed, the average values of $\cos 2\theta_{e1}$ and $\cos 4\theta_{e1}$ during one period are zero. Therefore, the average value of the system copper loss in the fault-tolerant operation can be calculated as (9).

B. Calculation Procedure of (10)

The five phase copper losses are calculated as follows:

$$\begin{cases} p_{b1} = i_{b1}^2R_s \\ p_{c1} = i_{c1}^2R_s \\ p_{a2} = i_{a2}^2R_s \\ p_{b2} = i_{b2}^2R_s \\ p_{c2} = i_{c2}^2R_s. \end{cases} \tag{B-1}$$

According to (13), the phase currents can be calculated as

$$\begin{cases} i_{b1} = i_{sd1}\cos(\theta_{e1}-2\pi/3)-i_{sq1}\sin(\theta_{e1}-2\pi/3) \\ i_{c1} = i_{sd1}\cos(\theta_{e1}+2\pi/3)-i_{sq1}\sin(\theta_{e1}+2\pi/3) \\ i_{a2} = i_{sd2}\cos(\theta_{e2})-i_{sq2}\sin(\theta_{e2}) \\ i_{b2} = i_{sd2}\cos(\theta_{e2}-2\pi/3)-i_{sq2}\sin(\theta_{e2}-2\pi/3) \\ i_{c2} = i_{sd2}\cos(\theta_{e2}+2\pi/3)-i_{sq2}\sin(\theta_{e2}+2\pi/3). \end{cases} \tag{B-2}$$

$$\begin{cases} i_{b1} = \frac{1}{\sqrt{3}}I_{m1}\sin 2\theta_{e1}\cos(\theta_{e1}-2\pi/3)-\frac{1}{\sqrt{3}}I_{m1} \\ \qquad (\cos 2\theta_{e1}+1)\sin(\theta_{e1}-2\pi/3) \\ i_{c1} = \frac{1}{\sqrt{3}}I_{m1}\sin 2\theta_{e1}\cos(\theta_{e1}+2\pi/3)-\frac{1}{\sqrt{3}}I_{m1} \\ \qquad (\cos 2\theta_{e1}+1)\sin(\theta_{e1}+2\pi/3) \\ i_{a2} = -[I_T-\frac{1}{\sqrt{3}}I_{m1}(1+\cos 2\theta_{e1})]\sin(\theta_{e2}) \\ i_{b2} = -[I_T-\frac{1}{\sqrt{3}}I_{m1}(1+\cos 2\theta_{e1})]\sin(\theta_{e2}-2\pi/3) \\ i_{c2} = -[I_T-\frac{1}{\sqrt{3}}I_{m1}(1+\cos 2\theta_{e1})]\sin(\theta_{e2}+2\pi/3) \end{cases} \tag{B-3}$$

$$\begin{cases} i_{b1} = \frac{1}{\sqrt{3}}I_T\eta\sin 2\theta_{e1}\cos(\theta_{e1}-2\pi/3)-\frac{1}{\sqrt{3}}I_T\eta \\ \qquad (\cos 2\theta_{e1}+1)\sin(\theta_{e1}-2\pi/3) \\ i_{c1} = \frac{1}{\sqrt{3}}I_T\eta\sin 2\theta_{e1}\cos(\theta_{e1}+2\pi/3)-\frac{1}{\sqrt{3}}I_T\eta \\ \qquad (\cos 2\theta_{e1}+1)\sin(\theta_{e1}+2\pi/3) \\ i_{a2} = -I_T[1-\frac{1}{\sqrt{3}}\eta(1+\cos 2\theta_{e1})]\sin(\theta_{e2}) \\ i_{b2} = -I_T[1-\frac{1}{\sqrt{3}}\eta(1+\cos 2\theta_{e1})]\sin(\theta_{e2}-2\pi/3) \\ i_{c2} = -I_T[1-\frac{1}{\sqrt{3}}\eta(1+\cos 2\theta_{e1})]\sin(\theta_{e2}+2\pi/3). \end{cases} \tag{B-4}$$

Substituting (5) and (6) into (B-2) gives (B-3). According to the definition "$\eta = I_{m1}/I_T$," (B-3) can be simplified as (B-4), which can be simplified as

$$\begin{cases} i_{b1} = I_T\,\eta\cos(\theta_{e1}) \\ i_{c1} = -I_T\,\eta\cos(\theta_{e1}) \\ i_{a2} = -I_T\,[1-(1/\sqrt{3})\eta\,(1+\cos 2\,\theta_{e1})]\sin(\theta_{e2}) \\ i_{b2} = -I_T[1-(1/\sqrt{3})\eta(1+\cos 2\,\theta_{e1})]\sin(\theta_{e2}-2\pi/3) \\ i_{c2} = -I_T[1-(1/\sqrt{3})\eta(1+\cos 2\,\theta_{e1})]\sin(\theta_{e2}+2\pi/3). \end{cases} \tag{B-5}$$

Based on (B-5), i_{b1}^2 and i_{c1}^2 can be calculated as

$$i_{b1}^2 = i_{c1}^2 = \frac{1+\cos(2\,\theta_{e1})}{2} I_T^2\eta^2. \tag{B-6}$$

For a nonzero rotor speed, the average value of $\cos 2\,\theta_{e1}$ during one period is zero. Therefore, the average value of i_{b1}^2 and i_{c1}^2 can be calculated as

$$\overline{i_{b1}^2} = \overline{i_{c1}^2} = \frac{1}{2} I_T^2\eta^2. \tag{B-7}$$

Based on (B-5), i_{a2}^2 can be calculated as (B-8). For a nonzero rotor speed, the average values of $\cos 2\,\theta_{e1}$, $\cos 4\theta_{e1}$, $\cos 2\,\theta_{e2}$, $\sin 4\theta_{e1}$, and $\cos 4\theta_{e1}\cos 2\,\theta_{e2}$ during one period are zero. Additionally, $\Delta\theta$ is a constant for a specific dual three-phase PMSM. Hence, the average value of i_{a2}^2 can be calculated as

$$\begin{aligned} i_{a2}^2 &= \frac{1}{12} I_T^2\,[(3-2\cos 2\Delta\theta)\eta^2 - 2\sqrt{3}(2-\cos 2\Delta\theta)\eta + 6] \\ &+ \frac{1}{2} I_T^2\left(\frac{2}{3}\eta^2\cos 2\,\theta_{e1} - \frac{2}{\sqrt{3}}\eta\cos 2\,\theta_{e1} + \frac{1}{6}\eta^2\cos 4\theta_{e1}\right) \\ &- \frac{1}{2} I_T^2\left(1-\frac{2}{\sqrt{3}}\eta+\frac{1}{2}\eta^2\right)\cos 2\,\theta_{e2} - \frac{1}{12} I_T^2\,\eta^2\cos 4\theta_{e1}\cos 2\,\theta_{e2} \\ &- \frac{1}{2} I_T^2\left(\frac{2}{3}\eta^2 - \frac{2}{\sqrt{3}}\eta\right)\left(\frac{1}{2}\cos 4\theta_{e1}\cos 2\Delta\theta - \frac{1}{2}\sin 4\theta_{e1}\sin 2\Delta\theta\right) \end{aligned} \tag{B-8}$$

$$\overline{i_{a2}^2} = \frac{1}{12} I_T^2\,[(3-2\cos 2\Delta\theta)\eta^2 - 2\sqrt{3}(2-\cos 2\Delta\theta)\eta + 6]. \tag{B-9}$$

Similarly, $\overline{i_{b2}^2}$ and $\overline{i_{c2}^2}$ can be obtained by (B-10). According to (B-7), (B-9), and (B-10), the average phase copper losses can be calculated by (12)

$$\begin{cases} \overline{i_{b2}^2} = \dfrac{I_T^2}{12}\{[3-2\cos(2\Delta\theta+2\pi/3)]\eta^2 - 2\sqrt{3}[2-\cos \\ \qquad (2\Delta\theta+2\pi/3)]\eta+6\} \\ \overline{i_{c2}^2} = \dfrac{I_T^2}{12}\{[3-2\cos(2\Delta\theta-2\pi/3)]\eta^2 - 2\sqrt{3}[2-\cos \\ \qquad (2\Delta\theta-2\pi/3)]\eta+6\}. \end{cases} \tag{B-10}$$

REFERENCES

[1] T. Sun and J. Wang, "Extension of virtual-signal-injection-based MTPA control for interior permanent-magnet synchronous machine drives into the field-weakening region," *IEEE Trans. Ind. Electron.*, vol. 62, no. 11, pp. 6809–6817, Nov. 2015.

[2] T. V. Frandsen, L. Mathe, N. I. Berg, R. K. Holm, T. N. Matzen, P. O. Rasmussen, and K. K. Jensen, "Motor integrated permanent magnet gear in a battery electrical vehicle," *IEEE Trans. Ind. Appl.*, vol. 51, no. 2, pp. 1516–1525, Mar./Apr. 2015.

[3] V. Ruuskanen, J. Nerg, J. Pyrhonen, S. Ruotsalainen, and R. Kennel, "Drive cycle analysis of a permanent-magnet traction motor based on magnetostatic finite-element analysis," *IEEE Trans. Veh. Technol.*, vol. 64, no. 3, pp. 1249–1254, Mar. 2015.

[4] W. Wang, M. Cheng, B. Zhang, Y. Zhu, and S. Ding, "A fault-tolerant permanent-magnet traction module for subway applications," *IEEE Trans. Power Electron.*, vol. 29, no. 4, pp. 1646–1658, Apr. 2014.

[5] P. B. Reddy, A. M. El-Refaie, and H. Kum-Kang, "Effect of number of layers on performance of fractional-slot concentrated-windings interior permanent magnet machines," *IEEE Trans. Power Electron.*, vol. 30, no. 4, pp. 2205–2218, Apr. 2015.

[6] W. Zhao, J. Zheng, J. Wang, G. Liu, J. Zhao, and Z. Fang, "Design and analysis of a linear permanent-magnet vernier machine with improved force density," *IEEE Trans. Ind. Electron.*, vol. 63, no. 4, pp. 2072–2082, Apr. 2016.

[7] J. Hang, J. Zhang, M. Cheng, and B. Zhang, "High-resistance connection detection in permanent magnet synchronous machine using zero-sequence current component," *IEEE Trans. Power Electron.*, vol. 31, no. 7, pp. 4710–4719, Jul. 2016.

[8] M. Cheng, J. Hang, and J. Zhang, "Overview of fault diagnosis theory and method for permanent magnet machine," *Chin. J. Electr. Eng.*, vol. 1, no. 1, pp. 21–36, Dec. 2015.

[9] A. Mohammadpour and L. Parsa, "Global fault-tolerant control technique for multiphase permanent-magnet machines," *IEEE Trans. Ind. Appl.*, vol. 51, no. 1, pp. 178–186, Jan./Feb. 2015.

[10] F. Immovilli, C. Bianchini, E. Lorenzani, A. Bellini, and E. Fornasiero, "Evaluation of combined reference frame transformation for interturn fault detection in permanent-magnet multiphase machines," *IEEE Trans. Ind. Electron.*, vol. 62, no. 3, pp. 1912–1920, Mar. 2015.

[11] E. Prieto-Araujo, A. Junyent-Ferr, D. Lavernia-Ferrer, and O. Gomis-Bellmunt, "Decentralized control of a nine-phase permanent magnet generator for offshore wind turbines," *IEEE Trans. Energy Convers.*, vol. 30, no. 3, pp. 1103–1112, Sep. 2015.

[12] E. Levi, "Multiphase electric machines for variable-speed applications," *IEEE Trans. Ind. Electron.*, vol. 55, no. 5, pp. 1893–1909, May 2008.

[13] R. Yuan and Z. Q. Zhu, "Enhancement of steady-state performance in direct-torque-controlled dual three-phase permanent-magnet synchronous machine drives with modified switching table," *IEEE Trans. Ind. Electron.*, vol. 62, no. 6, pp. 3338–3350, Jun. 2015.

[14] C. Zhou, G. Yang, and J. Su, "PWM strategy with minimum harmonic distortion for dual three-phase permanent-magnet synchronous motor drives operating in the overmodulation region," *IEEE Trans. Power Electron.*, vol. 31, no. 2, pp. 1367–1380, Feb. 2016.

[15] J. Karttunen, S. Kallio, P. Peltoniemi, P. Silventoinen, and O. Pyrhonen, "Decoupled vector control scheme for dual three-phase permanent magnet synchronous machines," *IEEE Trans. Ind. Electron.*, vol. 61, no. 5, pp. 2185–2196, May 2014.

[16] E. Mese, Y. Yasa, H. Akca, M. G. Aydeniz, and M. Garip, "Investigating operating modes and converter options of dual winding permanent magnet synchronous machines for hybrid electric vehicles," *IEEE Trans. Energy Convers.*, vol. 30, no. 1, pp. 285–295, Mar. 2015.

[17] J. O. Estima and A. J. M. Cardoso, "A fault-tolerant permanent magnet synchronous motor drive with integrated voltage source inverter open-circuit faults diagnosis," in *Proc. Eur. Conf. Power Electron. Appl.*, Birmingham, U.K., 2011, pp. 1–10.

[18] X. Jiang, W. Huang, R. Cao, Z. Hao, and W. Jiang, "Electric drive system of dual-winding fault-tolerant permanent-magnet motor for aerospace applications," *IEEE Trans. Ind. Electron.*, vol. 62, no. 12, pp. 7322–7330, Dec. 2015.

[19] B. A. Welchko, T. A. Lipo, T. M. Jahns, and S. E. Schulz, "Fault tolerant three-phase AC motor drive topologies: A comparison of features, cost, and limitations," *IEEE Trans. Power Electron.*, vol. 19, no. 4, pp. 1108–1116, Jul. 2004.

[20] A. Kontarcek, P. Bajec, M. Nemec, V. Ambrozic, and D. Nedeljkovic, "Cost-effective three-phase PMSM drive tolerant to open-phase fault," *IEEE Trans. Ind. Electron.*, vol. 62, no. 11, pp. 6708–6718, Nov. 2015.

[21] A. Gaeta, G. Scelba, and A. Consoli, "Modeling and control of three-phase PMSMs under open-phase fault," *IEEE Trans. Ind. Appl.*, vol. 49, no. 1, pp. 74–83, Jan./Feb. 2013.

[22] K. D. Hoang, Z. Q. Zhu, and M. Foster, "Direct torque control of permanent magnet brushless AC drive with single-phase open-circuit fault accounting for influence of inverter voltage drop," *IET Electr. Power Appl.*, vol. 7, no. 5, pp. 369–380, May 2013.

[23] Y. Xu, H. Yan, and J. Zou, "A fault-tolerant control strategy for six-phase transverse flux tubular PMLM based on synthetic vector method," *IEEE Trans. Plasma Sci.*, vol. 43, no. 5, pp. 1332–1338, May 2015.
[24] P. Delarue, A. Bouscayrol, and E. Semail, "Generic control method of multileg voltage-source-converters for fast practical implementation," *IEEE Trans. Power Electron.*, vol. 18, no. 2, pp. 517–526, Mar. 2003.
[25] L. Chee-Shen, E. Levi, M. Jones, N. Abd Rahim, and H. Wooi-Ping, "A fault-tolerant two-motor drive with FCS-MP-based flux and torque control," *IEEE Trans. Ind. Electron.*, vol. 61, no. 12, pp. 6603–6614, Dec. 2014.
[26] W. Wang, J. Zhang, and M. Cheng, "A dual-level hysteresis current control for one five-leg VSI to control two PMSMs," *IEEE Trans. Power Electron.*, to be published, doi: 10.1109/TPEL.2016.2535294.
[27] S. Ito, T. Moroi, Y. Kubo, K. Matsuse, and K. Rajashekara, "Independent control of two permanent-magnet synchronous motors fed by a four-leg inverter," *IEEE Trans. Ind. Appl.*, vol. 51, no. 1, pp. 753–760, Jan./Feb. 2015.
[28] K. Matsuse, N. Kezuka, and K. Oka, "Characteristics of independent two induction motor drives fed by a four-leg inverter," *IEEE Trans. Ind. Appl.*, vol. 47, no. 5, pp. 2125–2134, Sep./Oct. 2011.
[29] A. Bouscayrol, M. Pietrzak-David, P. Delarue, R. Pena-Eguiluz, P. E. Vidal, and X. Kestelyn, "Weighted control of traction drives with parallel-connected AC machines," *IEEE Trans. Ind. Electron.*, vol. 53, no. 6, pp. 1799–1806, Dec. 2006.
[30] M. A. Shamsi-Nejad, B. Nahid-Mobarakeh, S. Pierfederici, and F. Meibody-Tabar, "Fault tolerant and minimum loss control of double-star synchronous machines under open phase conditions," *IEEE Trans. Ind. Electron.*, vol. 55, no. 5, pp. 1956–1965, May 2008.

Wei Wang (S'10–M'14) was born in Jiangsu, China. He received the B.Sc. degree in electrical engineering from the Nanjing University of Science and Technology, Nanjing, China, in 2008, and the Ph.D. degree in electrical engineering from Southeast University, Nanjing, in 2014.

From October 2011 to October 2012, he got the scholarship from China Scholarship Council and was a joint Ph.D. Student with the University of Lille 1, Lille, France. Since 2014, he has been with Southeast University, where he is currently a Lecturer at the School of Electrical Engineering. He is the Author or Coauthor of more than 20 technical papers. His research interests include motor drives and traction system of rail transit.

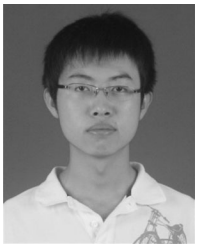

Jinghao Zhang was born in Gansu, China. He received the B.Sc. degree in electrical engineering from the Nanjing University of Science and Technology, Nanjing, China, in 2014. He is currently working toward the M.Sc. degree in electrical engineering at Southeast University, Nanjing.

His current research interests include electrical machine drive and traction system of rail transit.

Ming Cheng (M'01–SM'02–F'15) received the B.Sc. and M.Sc. degrees from the Department of Electrical Engineering, Southeast University, Nanjing, China, in 1982 and 1987, respectively, and the Ph.D. degree from the Department of Electrical and Electronic Engineering, University of Hong Kong, Hong Kong, in 2001.

From January to April 2011, he was a Visiting Professor with the Wisconsin Electric Machine and Power Electronics Consortium, University of Wisconsin, Madison, WI, USA. Since 1987, he has been with Southeast University, where he is currently a Distinguished Professor at the School of Electrical Engineering and the Director of the Research Center for Wind Power Generation. His teaching and research interests include electrical machines, motor drives for EV, and renewable energy generation. He has authored or coauthored more than 300 technical papers and four books, and is the holder of 70 patents in these areas.

Prof. Cheng is a Fellow of the Institution of Engineering and Technology. He has served as the Chair and an Organizing Committee Member for many international conferences. He is a Distinguished Lecturer of the IEEE Industry Applications Society for 2015/2016.

Shihua Li (A'05–M'06–SM'10) was born in Pingxiang, Jiangxi Province, China in 1975. He received the bachelor's, master's, and Ph.D. degrees in automatic control from Southeast University, Nanjing, China, in 1995, 1998, and 2001, respectively.

Since 2001, he has been with the School of Automation, Southeast University, where he is currently a Professor and the Director at the Mechatronic Systems Control Laboratory. He has authored or coauthored more than 200 technical papers and two books in these areas. His main research interests include modeling, analysis, and nonlinear control theory (nonsmooth control, disturbance rejection control, adaptive control, etc.) with applications to mechatronic systems, including manipulator, robot, ac motor, power electronic systems, and others.

Dr. Li is a Member of the Nonlinear Systems and Control Technical Committee, and the System Identification and Adaptive Control Technical Committee of the IEEE CSS, a Member of the Electrical Machines Technical Committee and the Motion Control Technical Committee of the IEEE IES. He serves as an Associate Editor or Editor for the *International Journal of Robust and Nonlinear Control*, the *IET Power Electronics*, the *International Journal of Electronics*, the *Journal of Power Electronic*, and Guest Editor of the IEEE TRANSACTIONS ON INDUSTRIAL ELECTRONICS, the *International Journal of Robust and Nonlinear Control*, and the *IET Control Theory and Applications*. He is the Vice Chairman of the IEEE CSS Nanjing Chapter.